nature physics

LETTERS

PUBLISHED ONLINE: 4 JULY 2010 | DOI: 10.1038/NPHYS1717

Zero-doping state and electron–hole asymmetry in an ambipolar cuprate

Kouji Segawa[1], M. Kofu[2], S-H. Lee[2], I. Tsukada[3], H. Hiraka[4], M. Fujita[4], S. Chang[5], K. Yamada[6]* and Yoichi Ando[1]*

A Mott insulator is a material that is insulating because of strong Coulomb repulsions between electrons. Doping charge carriers, electrons or holes into a Mott insulator can induce high-temperature superconductivity. Thus, what exactly happens when a charge carrier is doped into a Mott insulator is a key question in many-body physics[1–4]. To address this issue, ideally one should start from a zero-doping state[5–7] and be able to introduce both holes and electrons in the dilute limit. However, such an idealized experiment has been impossible because of the lack of suitable materials. Here we show that a new 'ambipolar' cuprate makes it possible for the first time to cross the zero-doping state in the same material, which in turn allows us to address the physics of the extremely low-doping region. Surprisingly, we found that the antiferromagnetic ground state sharply changes between electron- and hole-doped sides, and this change is dictated by the existence of only 0.1 ppm of charge carriers. Moreover, we observed that the Néel temperature T_N shows an unexpected reduction in a narrow range centred at the zero-doping state, across which the system exhibits asymmetric behaviours in transport measurements. Our findings reveal the inherently different nature of electron and hole doping in the dilute limit of a Mott-insulating cuprate.

Most of the cuprate superconductors are either uniquely hole-doped (p-type) as in $La_{2-x}Sr_xCuO_4$, $YBa_2Cu_3O_y$ and $Bi_2Sr_2CaCu_2O_{8+\delta}$ or electron-doped (n-type) as in $Ln_{2-x}Ce_xCuO_4$ (Ln = Nd, Pr). The main structural difference is the lack of apical oxygens in the n-type cuprates[4,8]. Recently a system has been found where the sign of the charge carriers can be flipped without altering the crystal structure[9]. In $Y_{1-z}La_z(Ba_{1-x}La_x)_2Cu_3O_y$ (YLBLCO), the substitution of La for Ba provides electrons and, for $x = 0.13$ and $z = 0.62$, the charge carriers can be controlled[9] from 7% of holes per planar Cu (superconducting below 25 K) to 2% of electrons (non-superconducting) through the zero-doping state, by simply changing the oxygen content, which is done by removing oxygen from the Cu–O chain site; there is no difference in the chemical procedure for p- and n-type doping. Figure 1 shows the crystal structure and the scheme of chemical doping in YLBLCO, together with a generalized phase diagram of the cuprates. Note that in YLBLCO the apical oxygen is intact even in the n-type regime. To the best of our knowledge, YLBLCO is so far the only ambipolar cuprate that provides a unique opportunity to investigate the extremely low-doping region around the Mott insulating boundary spanning both p- and n-type regimes.

Let us begin by showing how the resistivity changes on ambipolar doping. Figure 2a–c shows the temperature dependence of the c-axis resistivity, ρ_c, for various oxygen contents in YLBLCO from $y = 6.22$ to 6.80, measured up to 500 K. The highest value of ρ_c at room temperature is achieved for $y = 6.32$: $\rho_c(300\,\mathrm{K}) \simeq 10^5\,\Omega\,\mathrm{cm}$, which is unprecedented for cuprates. This suggests that the real boundary between n- and p-type cuprates, which is defined as the Mott-insulating state, is close to $y = 6.32$. ρ_c does not change much for $y = 6.31$–6.36 (Fig. 2b), and it starts to decrease for $y < 6.31$ (Fig. 2c) due to the conductance of electron carriers[9]. A recent X-ray photoemission spectroscopy study[10] clearly showed a chemical potential jump at $y \sim 6.32$ when y decreases, which confirms the change of carrier type at $y \sim 6.32$. Furthermore, a change in the Cu 2p X-ray photoemission spectroscopy peaks has been observed, which indicates that the electron doping indeed results in carriers in the CuO_2 planes[10].

On close examination, it can be seen that $\rho_c(T)$ exhibits a weak kink at each doping concentration. The anomaly can be seen more clearly, as either a peak or a dip, when the normalized temperature derivative of $\rho_c(T)$, $(d\rho/dT)/\rho$, is plotted in Fig. 2d–f. The dip, observed in p-type samples with $y \geq 6.32$ (Fig. 2d,e), is similar to the dip observed[11] in the pristine $YBa_2Cu_3O_y$. On the other hand, in n-type samples ($y \leq 6.30$) a peak rather than a dip is observed (Fig. 2f). Below, our neutron scattering data will show that the anomaly is associated with magnetic ordering. However, the different kinks suggest an asymmetry between p- and n-type cuprates in the transport properties. Before we discuss the doping dependence of the transport properties, let us discuss how the magnetic ground state evolves when the nature of the charge carriers changes near the Mott critical point, $y = 6.32$.

Elastic neutron scattering measurements were carried out on the same crystals as used in the $\rho_c(T)$ measurements. Figure 3a–f shows the data taken along the $[0.5, 0.5, L]$ direction centred at $L = 1$ and 1.5. For the electron-doped (n-type) sample with an oxygen content of $y = 6.22$, at 7 K a sharp peak exists at the half-integer L (Fig. 3d), and no signal exists at the integer L (Fig. 3a). For the hole-doped (p-type) sample with $y = 6.69$, on the other hand, no peak was observed at the half-integer L (Fig. 3f) and instead a peak appeared at the integer L (Fig. 3c). The magnetic ordering in both compositions occurs at ~360 K (Fig. 3g,i), which is consistent with the temperature where $\rho_c(T)$ and $d\rho_c/dT$ show the anomaly. The magnetic Bragg peaks were measured at several different corresponding wave vectors with half-integer Ls for $y = 6.22$ and with integer Ls for $y = 6.69$, and their relative

[1]Institute of Scientific and Industrial Research, Osaka University, Ibaraki, Osaka 567-0047, Japan, [2]Department of Physics, University of Virginia, Charlottesville, Virginia 22904-4714, USA, [3]Central Research Institute of Electric Power Industry, Yokosuka, Kanagawa 240-0196, Japan, [4]Institute for Materials Research, Tohoku University, Sendai, 980-8577, Japan, [5]NIST Center for Neutron Research, National Institute of Standards and Technology, Gaithersburg, Maryland 20899, USA, [6]Advanced Institute for Materials Research, Tohoku University, Sendai, 980-8577, Japan.
*e-mail: kyamada@imr.tohoku.ac.jp; y_ando@sanken.osaka-u.ac.jp.

© 2010 Macmillan Publishers Limited. All rights reserved.

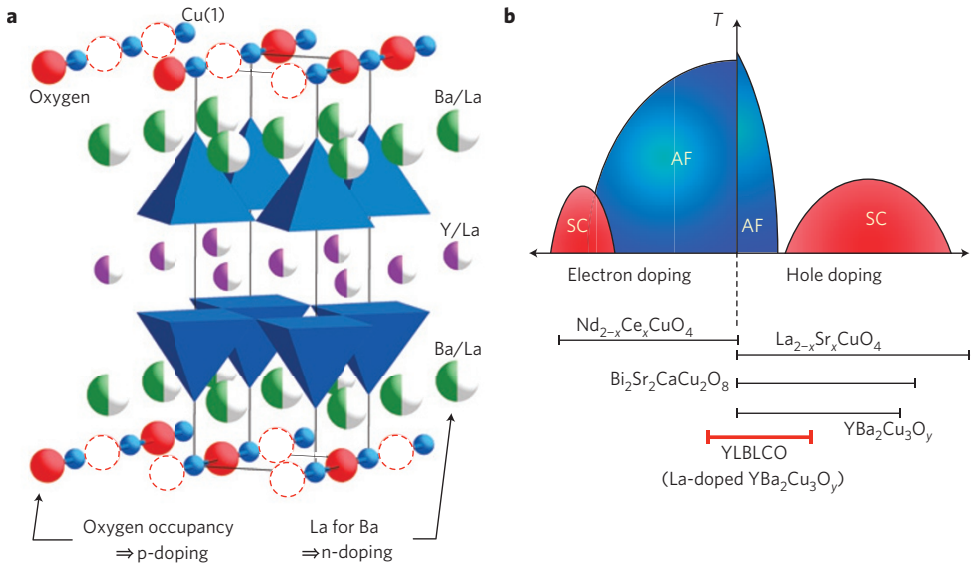

Figure 1 | Schematics of YLBLCO. a, Crystal structure of YLBLCO and the sites for chemical doping. Note that in actual YLBLCO the Cu–O chains are fragmented and randomly oriented, leading to a macroscopically tetragonal structure. **b**, Generalized phase diagram of cuprate materials, where AF and SC denote antiferromagnetic and superconducting regions, respectively. Attainable doping ranges are shown for several cuprate materials including YLBLCO.

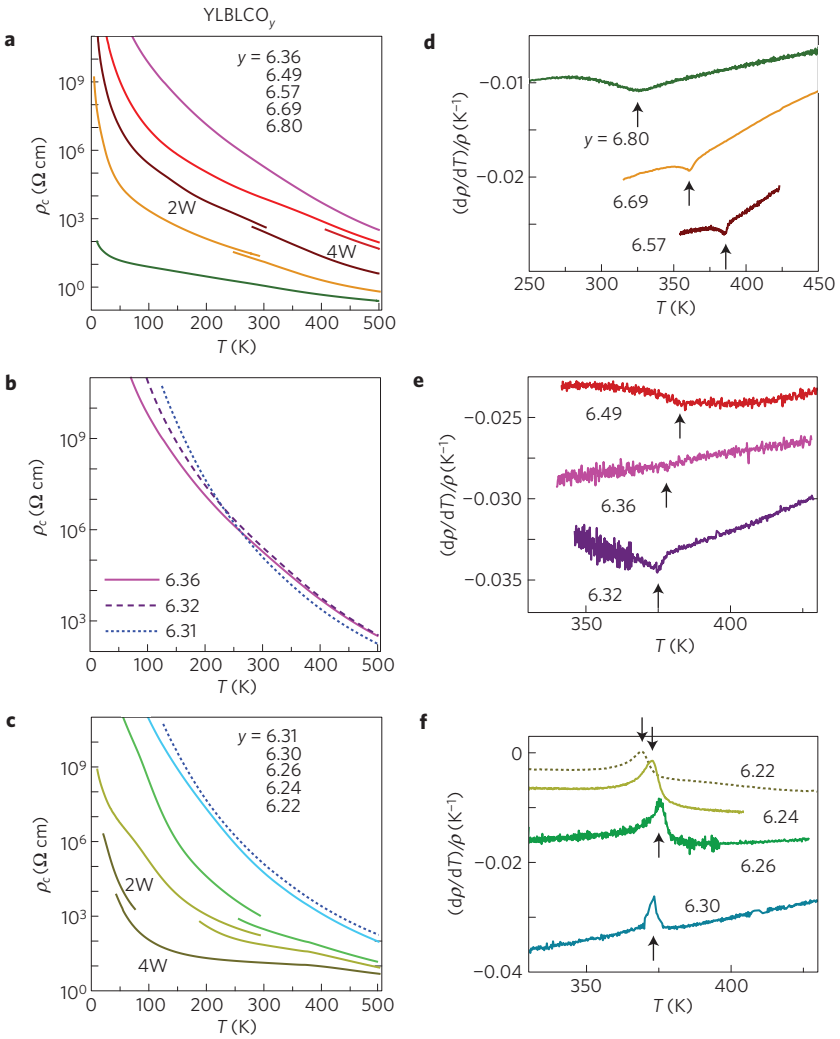

Figure 2 | Temperature dependence of ρ_c. a–c, $\rho_c(T)$ of YLBLCO in semi-log plots, where 4W (four-wire) and 2W (two-wire) denote the methods for resistivity measurements. **d–f**, Temperature derivative of $\rho_c(T)$ normalized by ρ_c. The arrows indicate the position of the peak or the dip, at which the Néel transition is supposed to take place.

© 2010 Macmillan Publishers Limited. All rights reserved.

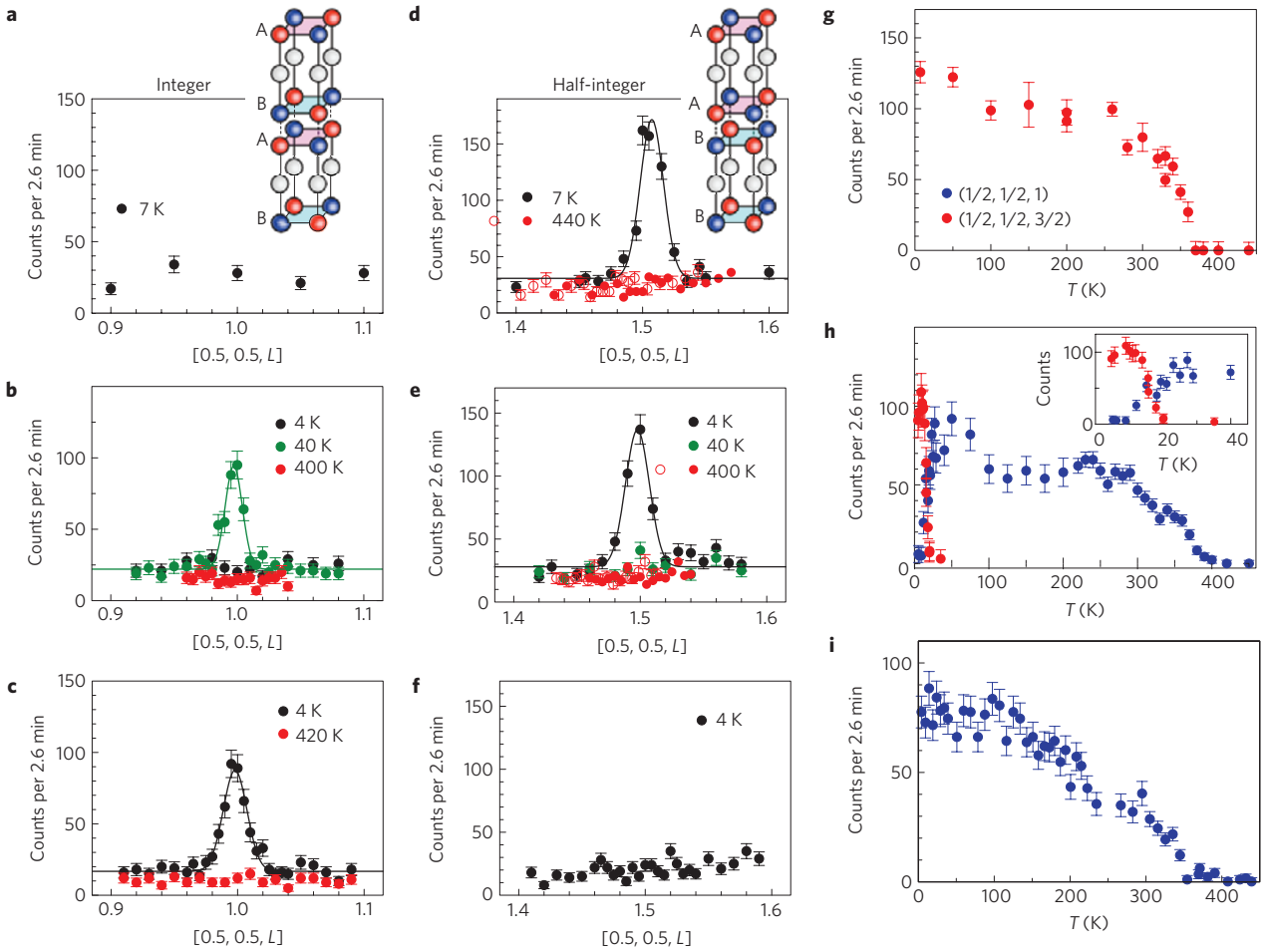

Figure 3 | Magnetic ground states of YLBLCO studied by neutron scattering. a–f, Neutron scattering intensities obtained by [0.5, 0.5, *L*] scans for $y = 6.22$ (electron doped) (**a**,**d**), $y = 6.32$ (nearly zero doping) (**b**,**e**) and $y = 6.69$ (hole doped) (**c**,**f**) at different temperatures. The insets show schematics of the magnetic structures of YLBLCO for respective regimes. The red and blue spheres at the Cu(2) sites stand for spins with opposite directions (the exact direction of the spin easy axis is unknown), and grey spheres are the Cu(1) atoms. The small (or negligible) moments of the Cu(1) atoms are not plotted. The letters A and B denote the difference (π-phase shift) in spin arrangements in the plane. **g–i**, Temperature dependencies of the integrated intensity of the magnetic reflections for $y = 6.22$ (**g**), 6.32 (**h**) and 6.69 (**i**). The inset to **h** magnifies the low-temperature data for $y = 6.32$. The error bars represent one standard deviation.

intensities were used to determine their magnetic ground-state structures. For both compositions, the magnetic moments at the Cu sites in the CuO_2 planes (called Cu(2)) are antiferromagnetically ordered in the horizontal-plane with an ordered moment $\langle M \rangle$ of $\sim 0.3\,\mu_B$/Cu(2), represented by red and blue spheres in the insets of Fig. 3a,d. The orientation of the moments, on the other hand, could not be determined within our experimental accuracy (see the Supplementary Information for details). The Cu bilayers are coupled antiferromagnetically in both cases, and when translated by one lattice unit along the *c* axis the moments change sign for the n-type samples whereas they are the same for the p-type ones. The moments at the Cu sites in the Cu–O-chain layers (called Cu(1)) were small or negligible: $\langle M \rangle_{Cu(1)} \sim 0.04\mu_B$/Cu(1) and 0.00 μ_B/Cu(1) for $y = 6.22$ and 6.69, respectively.

To confirm that the observed magnetic structures are the generic ground states for the n- and p-type YLBLCO and to study how one magnetic structure evolves into another when the oxygen concentration increases, we carried out similar measurements on YLBLCO ($y = 6.32$). The oxygen content of $y = 6.32$ was chosen because this is the closest to the Mott critical point that separates the n- and p-type regions; indeed, the Hall coefficient R_H shows a sign change across this composition (see Fig. 4b). As shown in Fig. 3b,e,h, in this case on cooling the integer *L* peak first develops below $\sim$370 K but on further cooling it starts to decrease at $\sim$20 K below which the half-integer *L* peak appears. A similar change in the magnetic structure on cooling was observed in Nd_2CuO_4 where the ordering of Nd moments and the Nd–Cu interactions at low temperatures induce a second magnetic transition[12]. For YLBLCO ($y = 6.32$), the ordered moments of the Cu(2) sites were $\sim$0.24 and 0.26 μ_B/Cu(2) for the half-integer *L* and the integer *L* phase, respectively, whereas those of the Cu(1) sites were 0.002 and 0.00 μ_B/Cu(1) for the half-integer *L* and the integer *L* phase, respectively (see the Supplementary Information for details.) In the present case, the interaction between the moment on Cu(1) and Cu(2) is likely to be responsible for the spin reorientation similar to the case of Nd_2CuO_4. Besides, the crossover from the integer *L* to the half-integer *L* peak on cooling probably indicates that the sign of the dominant charge carriers in the $y = 6.32$ sample changes at $\sim$20 K, although R_H could not be measured on this sample because of a very high impedance. This also indicates that the observed magnetic structures are indeed the generic ground states for the electron- and hole-doped YLBLCO.

What causes the magnetic ground state to change abruptly when the sign of the charge carrier changes? We can rule out any crystal structural origin because no abrupt change in the crystal structure including the lattice constants was found at the n-to-p-type crossover. Experimentally, it seems that the magnetic

© 2010 Macmillan Publishers Limited. All rights reserved.

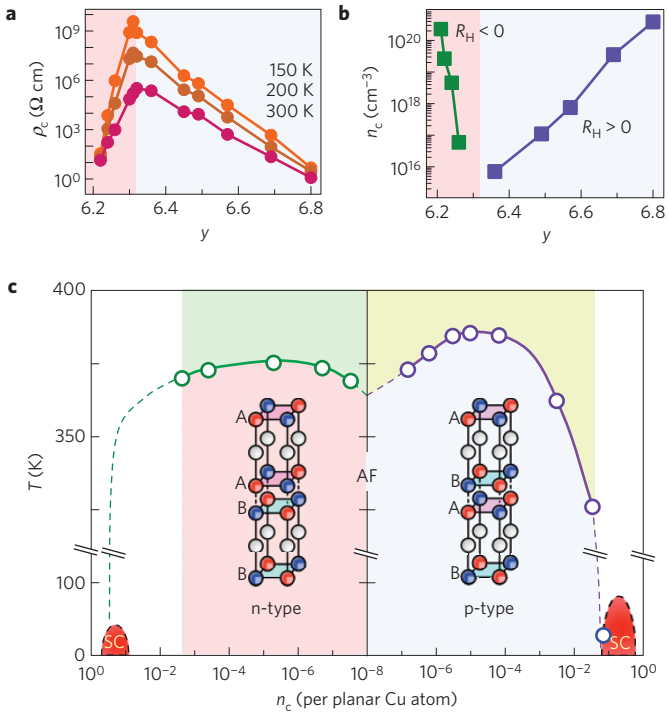

Figure 4 | Evolution of key parameters in YLBLCO. a, ρ_c shows a peak at $y = 6.32$, signifying the zero-doping point. **b**, The carrier concentration decreases exponentially towards the zero-doping point as y is varied; here, the R_H data at 300 K are used for the calculations, except for $y = 6.36$ and 6.49 for which 350 K data are used. Light red and blue backgrounds denote the n- and p-type regimes, respectively. The carrier mobility along the c axis calculated from these data is 10^{-3}–10^{-2} cm^2 V^{-1} s^{-1} and is nearly independent of both the concentration and the type of carriers. **c**, T_N as a function of the concentration of both p- and n-type carriers (solid lines are guides to the eye), together with the anticipated phase boundary for the regimes not covered in this study (dashed lines). Note that the horizontal axis is plotted in a logarithmic scale, and the region studied here is highlighted with light colours. T_N is extracted from the $\rho_c(T)$ data shown in Fig. 2d–f. The carrier concentrations for $y = 6.30$, 6.31 and 6.32 are estimated from ρ_c by extrapolating the relationship between ρ_c and R_H.

moments at the Cu(1) sites in the Cu–O-chain layers play a crucial role in selecting the particular magnetic ground state. For $y = 6.22$ (n-type), the small but non-zero moments at the Cu(1) planes would favour the observed $\mathbf{Q}_m = (0.5, 0.5, 0.5)$ magnetic structure along the c axis if they are coupled antiferromagnetically with the neighbouring Cu(2) layers. For $y = 6.69$ (p-type), on the other hand, the non-magnetic Cu(1) layers would not have such an effect, leading to the observed $\mathbf{Q}_m = (0.5, 0.5, 1)$ magnetic structure[13]. Note that the Cu(1) ions become magnetically ordered when excess electrons are doped rather than when excess holes are doped, even though the electron doping would decrease the number of magnetic Cu^{2+} ions at the Cu(1) site[14]. The observed magnetic ground states for the p- and n-type regimes may provide a possible explanation for why $d\rho_c/dT$ at T_N shows a dip (increase in ρ_c below T_N) for the p-type and a 'peak' for the n-type (decrease in ρ_c below T_N) (Fig. 2d–f): in the p-type magnetic structure, when a carrier hops from one bilayer to another bilayer it sees opposite Cu spins (see the inset of Fig. 3a), whereas in the n-type magnetic structure it sees parallel Cu spins (inset of Fig. 3d). Thus, a sort of 'spin-valve effect' may yield[15] a higher hopping probability for the n-type than for the p-type, which is consistent with our transport data.

In Fig. 4a, ρ_c is plotted as a function of the oxygen content at three different temperatures. It clearly shows that YLBLCO realizes the Mott-insulating state at $y \simeq 6.32$. When electrons are added or subtracted from this Mott state, ρ_c decreases but with a faster rate for n-type cuprates and a slower rate for p-type cuprates. The carrier concentration n_c calculated from the Hall coefficient R_H is plotted in Fig. 4b as a function of y, which confirms both the sign change of the main carriers near $y = 6.32$ and the different rate of charge transfer for the two regimes. It is interesting that this doping asymmetry seems to mimic the spectral-weight-transfer asymmetry expected for cuprates: because the cuprates are charge-transfer-type Mott insulators[16], the valence and conduction bands are primarily oxygen and copper bands, and their spectral weights are $2N$ and N, respectively, if the system has N cells (this is because the original spectral weight $2N$ of copper is split into the upper and lower Hubbard bands as a result of the on-site repulsion U); when an electron is added to the insulating state, in the localized limit it creates one doubly occupied copper site on which the two electrons have the same energy, so the new filled state has the spectral weight of two, whereas that of both the upper and lower Hubbard bands becomes $N - 1$; on the other hand, doping a hole simply reduces the spectral weight of the oxygen band to $2N - 1$. This means that the rate of the spectral-weight transfer on doping is twice as quick for electron doping, which is an inherent asymmetry[16] in the localized limit. The observed doping-rate asymmetry (Fig. 4a,b) may be related to the fundamental spectral-weight-transfer asymmetry in Mott-insulating cuprates.

Figure 4c shows the n_c-versus-T_N phase diagram of YLBLCO. In the n-type regime, the half-integer L magnetic state is stable over a very wide range of n_c spanning five orders of magnitude, with the maximum T_N at $n_c \sim 10^{-5}$ per planar Cu atom. When n_c approaches the zero-doping Mott-insulator point, T_N decreases. When the charge carrier becomes p-type, T_N starts increasing again as n_c increases up to $\sim 10^{-5}$ per planar Cu atom beyond which T_N decreases. The unexpected dip in T_N at the zero-doping point cannot be explained by a simple argument. Furthermore, the magnetic structure changes between p- and n-types in response to as small as 0.1 ppm of carriers, which is surprising. The 'competition' between the two magnetic structures, which can be inferred in the $y = 6.32$ sample in its temperature dependence, may be responsible for the observed intriguing phenomena near the zero-doping state. Clearly, the physics of very dilute carriers in Mott insulators is more intricate than expected, and its understanding may help disentangle the complex physics[17] of the cuprates.

Methods

Single crystals of YLBLCO are grown by a flux method using 99.9%-pure Y_2O_3 crucibles. The chemical composition of the grown crystals is analysed by inductively coupled plasma atomic emission spectroscopy, which gives $z = 0.62$ and $x = 0.13$. The carrier concentration in YLBLCO can be controlled from ~2% of n-type carriers to ~7% of p-type ones through the Mott insulator by changing the oxygen content y from 6.21 to 6.95 (ref. 9). Reducing y to below 6.21 results in decomposition of the crystal. ρ_c is measured by the four-wire method for resistance below ~100 kΩ, and by the two-wire method for higher resistance up to ~10^{11} Ω, where an electrometer is used with the guarding technique. All of the measurements of ρ_c are carried out on the same two crystals while varying the oxygen content; removable electrodes are used and the crystals are reannealed after each measurement. The error in the absolute value of the resistivity in the two crystals is within 20% for the four-wire method, and 50% for the two-wire method. The Hall coefficient is measured by sweeping the magnetic field applied along the c axis up to 7 T, and the error can be up to 20% for high-resistance compositions. The elastic neutron scattering measurements were carried out on the cold neutron triple-axis spectrometer SPINS at the National Institute of Standards and Technology. The neutron energy was fixed at 3.7 meV. Contamination from higher-order beams was effectively eliminated using Be and BeO filters before and after the sample, which was $0.5 \times 0.5 \times 0.2$ mm^3 in size. For each sample, elastic scans were carried out at several different magnetic Bragg reflections. The integrated intensities were normalized in an absolute unit using the integrated intensity of the nuclear (003) Bragg reflection, and used for determining the magnetic moments of the Cu(1) and Cu(2) ions. See the Supplementary Information for details.

© 2010 Macmillan Publishers Limited. All rights reserved.

Received 19 January 2010; accepted 2 June 2010; published online 4 July 2010

References

1. Dagotto, E. Correlated electrons in high-temperature superconductors. *Rev. Mod. Phys.* **66,** 763–840 (1994).
2. Lee, P. A., Nagaosa, N. & Wen, X-G. Doping a Mott insulator: Physics of high-temperature superconductivity. *Rev. Mod. Phys.* **78,** 17–85 (2006).
3. Phillips, P. Colloquium: Identifying the propagating charge modes in doped Mott insulators. *Rev. Mod. Phys.* **82,** 1719–1742 (2010).
4. Imada, M., Fujimori, A. & Tokura, Y. Metal–insulator transitions. *Rev. Mod. Phys.* **70,** 1039–1263 (1998).
5. Kastner, M. A., Birgeneau, R. J., Shirane, G. & Endoh, Y. Magnetic, transport, and optical properties of monolayer copper oxides. *Rev. Mod. Phys.* **70,** 897–928 (1998).
6. Basov, D. N. & Timusk, T. Electrodynamics of high-T_c superconductors. *Rev. Mod. Phys.* **77,** 721–779 (2005).
7. Ono, S., Komiya, S. & Ando, Y. Strong charge fluctuations manifested in the high-temperature Hall coefficient of high-T_c cuprates. *Phys. Rev. B* **75,** 024515 (2007).
8. Armitage, N. P., Fournier, P. & Greene, R. L. Progress and perspectives on the electron-doped cuprates. *Rev. Mod. Phys.* (in the press); preprint at http://arxiv.org/abs/0906.2931 (2009).
9. Segawa, K. & Ando, Y. Doping n-type carriers by La-substitution for Ba in $YBa_2Cu_3O_y$ system. *Phys. Rev. B* **74,** 100508 (2006).
10. Ikeda, M. *et al.* Chemical potential jump between hole- and electron-doped sides of ambipolar high-T_c cuprate. Preprint at http://arxiv.org/abs/1001.0102 (2009).
11. Lavrov, A. N., Ando, Y., Segawa, K. & Takeya, J. Magnetoresistance in heavily underdoped $YBa_2Cu_3O_{6+x}$: Antiferromagnetic correlations and normal-state transport. *Phys. Rev. Lett.* **83,** 1419–1422 (1999).
12. Matsuda, M. *et al.* Three-dimensional magnetic structures and rare-earth magnetic ordering in Nd_2CuO_4 and Pr_2CuO_4. *Phys. Rev. B* **42,** 10098–10107 (1990).
13. Tranquada, J. M. *et al.* Neutron-diffraction determination of antiferromagnetic structure of Cu ions in $YBa_2Cu_3O_{6+x}$ with $x = 0.0$ and 0.15. *Phys. Rev. Lett.* **60,** 156–159 (1988).
14. Jorgensen, J. D. *et al.* Structural properties of oxygen-deficient $YBa_2Cu_3O_{7-\delta}$. *Phys. Rev. B* **41,** 1863–1877 (1990).
15. Thio, T. *et al.* Antisymmetric exchange and its influence on the magnetic structure and conductivity of La_2CuO_4. *Phys. Rev. B* **38,** 905–908 (1988).
16. Meinders, M. B., Eskes, H. & Sawatzky, G. A. Spectral-weight transfer: Breakdown of low-energy-scale sum rules in correlated systems. *Phys. Rev. B* **48,** 3916–3926 (1993).
17. Bonn, D. A. Are high-temperature superconductors exotic? *Nature Phys.* **2,** 159–168 (2006).

Acknowledgements

We thank E. Dagotto, P. Phillips and T. Tohyama for discussions. This work was supported by KAKENHI Grant Nos 19674002, 20030004, 19340090, 19540358 and 20740196. Works at UVA and at NCNR were supported by US DOE (BES-DMSE) Award No. DE-FE02-07ER46384 and NSF Award No. DMR-0454672, respectively.

Author contributions

All authors made critical comments on the manuscript. Y.A., K.S., S-H.L. and K.Y. contributed to planning of the experiments. K.S. synthesized the sample and carried out the transport measurements. K.S. and Y.A. analysed and interpreted the transport data. M.K., S-H.L., H.H., M.F., S.C. and K.Y. contributed to data collection of the neutron scattering. M.K., S-H.L. and K.Y. contributed to analysing the neutron data.

Additional information

The authors declare no competing financial interests. Supplementary information accompanies this paper on www.nature.com/naturephysics. Reprints and permissions information is available online at http://npg.nature.com/reprintsandpermissions. Correspondence and requests for materials should be addressed to Y.A. or K.Y.

© 2010 Macmillan Publishers Limited. All rights reserved.